Energy & Environmental Science

ROYAL SOCIETY OF CHEMISTRY

PAPER

View Article Online
View Journal | View Issue



Cite this: *Energy Environ. Sci.*, 2025, **18**, 6714

# Solid-state n-type thermodiffusion-assisted thermogalvanic cells with unprecedented thermal energy conversion†

Jeong-Ye Baek, [a] Hae Jin Seog[a] and Sung-Yeon Jang *[ab]

Thermogalvanic (TG) cells are a promising technology for harvesting low-grade waste heat, but their practical applications have been hindered by low thermopower and output power density. Here, we report for the first time a solid-state n-type thermodiffusion (TD)-assisted TG cell based on a PEDOT:PSS/$Fe(ClO_4)_{2/3}$ polymer complex. The strategic design of the polymer complex, featuring electrostatic interactions between the PEDOT:PSS matrix and the $Fe^{2+/3+}$ ions, enables the liberation of $ClO_4^-$ ions, enhancing thermodiffusion and ionic conductivity. This mechanism results in a remarkable ionic Seebeck coefficient of −40.05 mV $K^{-1}$ and a record-high normalized maximum power density of 56.57 mW $m^{-2}$ $K^{-2}$. The TD-assisted TG cell demonstrates excellent stability for >50 charge–discharge cycles. A 16-paired TG module generates 360 μW, sufficient to power commercial electronic devices. A wearable device showcases the practical applicability by harvesting body heat and producing 1.5 V. These findings represent a significant advancement in thermal energy harvesting and pave the way for practical TG-based energy conversion technologies.

Received 2nd March 2025,
Accepted 21st May 2025

DOI: 10.1039/d5ee01216c

rsc.li/ees



**Broader context**

The thermal energy conversion is crucial for sustainable energy solutions, as it enables the utilization of wasted heat from industrial processes, electronics, and the human body, transforming it into usable power. Thermogalvanic (TG) cells have attracted attention for their potential to harness energy from low-grade waste heat (<100 °C). However, the thermopower and output power density of TG cells have remained insufficient for practical self-powered devices. In this study, high thermopower solid-state n-type thermodiffusion-assisted TG cells were developed by designing a polymer complex—a polyelectrolyte combined with a galvanic couple—to enable constructive thermodiffusion and TG effects, leading to a substantial increase in output power density. The 16-paired TG modules, capable of delivering adequate power output, were successfully fabricated, allowing for the practical operation of commercial devices. Furthermore, a wearable device composed of 100 serially connected TG elements, arranged in a modular "Lego-like" design, effectively harvested body heat to generate 1.5 V. Our findings hold potential for applications across wearable and portable electronics, where efficient low-grade heat energy harvesting is essential.

## Introduction

In pursuit of high-energy density thermal energy conversion,[1] thermogalvanic (TG) cells have received significant attention for their potential use in energy harvesting from low-grade waste heat (<100 °C).[2,3] TG cells generate the thermopower based on the reversible electrochemical (faradaic) reaction of the galvanic couples.[2,4–7] Upon the subjection of a temperature gradient, the electrochemical reactions toward higher entropy are thermodynamically favored at the hot electrodes, whereas the reactions toward lower entropy are favored at the cold electrodes, generating a potential between the two electrodes. The products at each electrode are transported across the cell and then resupplied as the reactants at the counter electrodes, realizing continuous power generation.[8–10]

The improvement of power density in TG cells has primarily been investigated in the liquid-type cells, which can contain high concentrations of galvanic couples in aqueous media, demonstrating a thermopower of a few mV $K^{-1}$.[11,12] Nevertheless, the thermopower and output power density ($P_{out}$) from the TG cells have been relatively low for practical self-powering applications such as health monitors and smartwatches. Extensive research to improve the thermopower of TG cells has been reported by (i) enhancing the difference in redox reaction entropy ($\Delta s_{reaction}$) using additives and organic solvents[12–14] or (ii) improving the

[a] *School of Energy and Chemical Engineering, Ulsan National Institute of Science and Technology (UNIST), Ulsan, Republic of Korea. E-mail: syjang@unist.ac.kr*
[b] *Graduate School of Carbon Neutrality, Ulsan National Institute of Science and Technology (UNIST), Ulsan, Republic of Korea*

† Electronic supplementary information (ESI) available. See DOI: https://doi.org/10.1039/d5ee01216c

concentration gradient of redox species ($\Delta C_{redox}$) through thermally induced crystallization of redox species or gelation of the polymer matrix.[9,11] However, the improvement of the ionic Seebeck coefficient ($S_i$) of the TG cells was not significant. Moreover, there have been other intrinsic limitations for applying TG cells, such as solvent leakage in liquid-state cells and slow ion transportation in quasi-solid-state cells.[15–21]

Recently, a strategy that can enhance the $S_i$ of TG cells by utilizing additional ions has been reported.[22–24] For example, the addition of $K^+$ in TG cells based on a galvanic couple ($K_3Fe(CN)_6$/$K_4Fe(CN)_6$) containing a gelatin matrix substantially improved the $S_i$ value from 4.8 to 17 mV $K^{-1}$ because the thermodiffusion and cumulation of $K^+$ at the cold side increased the difference in the Eastman entropy of transfer ($\hat{S}_i$). However, the excess slow-diffusing $K^+$ in the quasi-solid gelatin matrix increased the internal resistance of the cells, resulting in a relatively low total $P_{out}$ (0.66 mW $m^{-2}$ $K^{-2}$).[22] The enhancement in $S_i$ and $P_{out}$ of the TE cells is essential for realistic applications.

In this work, high thermopower solid-state n-type thermodiffusion (TD)-assisted TG cells were developed by designing the polymer complex; a polyelectrolyte with a galvanic couple that can achieve the thermodiffusion and TG effects constructively. PEDOT:PSS was employed as the solid-state polyelectrolyte matrix, and $Fe(ClO_4)_{2/3}$ was selected as the galvanic couple. The interaction between $SO_3^-$ groups in the PEDOT:PSS and the multivalent $Fe^{2+/3+}$ cations in the galvanic couple physically crosslinks the polymer chains, liberating the counter ion ($ClO_4^-$). The thermodiffusion of the free $ClO_4^-$ ions in the polymer complex significantly enhanced the $S_i$, while providing ionic conduction channels to promote ion conductivity ($\sigma_i$) (Fig. S1 and Table S1, ESI†). Moreover, the acidic environment of PEDOT:PSS prevented the hydrolysis of $Fe^{2+/3+}$ to $Fe(OH)^+/^{2+}$, maintaining the charges of redox species, which is beneficial for maintaining $S_i$. This unique mechanism of the solid-state TD-assisted TG cells realized a remarkable $S_i$ of $-40.05$ mV $K^{-1}$ and $P_{max}/(\Delta T)^2$ of 56.57 mW $m^{-2}$ $K^{-2}$, representing a significant improvement compared to previous reports. Notably, this is the first report of a high-performance solid-state n-type TD-assisted TG cell. The 16-paired TG modules with $P_{out}$ of 360 μW were successfully fabricated, realizing the practical operation of commercial devices. Moreover, the wearable device, as constructed using 100 serially connected elements in a Lego-like design, successfully harvested body heat to produce 1.5 V.

## Results and discussion

### Design and working mechanism of the TD-assisted TG polymer complex

Fig. 1a demonstrates the operational principles of the solid-state TD-assisted TG cell introduced in this study. The $Fe(ClO_4)_{2/3}$ containing PEDOT:PSS (hereafter, PEDOT:PSS/$Fe(ClO_4)_{2/3}$) was used as the active TG material. When a temperature gradient is applied across the two Au electrodes, the redox reaction of the $Fe^{2+/3+}$ ions induces an electrochemical potential generating faradaic currents. Concurrently, electrostatic interaction between the $PSS^-$ and the $Fe^{2+/3+}$ ions prompts the dissociation of $ClO_4^-$ ions from the complex. The liberated $ClO_4^-$ ions migrate towards the colder electrode, contributing to the generation of electrical potential (electromotive force) (Fig. S2, ESI†) and capacitive (non-faradaic) currents, as depicted in Fig. 1b and c. This mechanism marks a pioneering approach in TG cell technology, distinct from prior methods, which incorporated additional ions to increase $S_i$ but suffered from reduced $P_{out}$ due to high internal resistance, as shown in Fig. S3 (ESI†).[15,18,22,25–28] The dual functionality of the galvanic couple in our TD-assisted TG material synergistically promotes both electrochemical reactions through $Fe^{2+/3+}$ and thermodiffusion *via* the liberated $ClO_4^-$ ions. The unique assembly of the polymer complex, featuring sulfonate functional groups ($R\text{-}SO_3^-$) capable of electrostatically interacting with the galvanic ions ($Fe^{2+/3+}$), facilitates the liberation of $ClO_4^-$ ions, while the unbound $Fe(ClO_4)_{2/3}$ continues to exhibit the TG effect.

The temperature coefficient of the galvanic couple, $Fe(ClO_4)_{2/3}$, at 0.3 M in deionized water, was measured to be 1.48 mV $K^{-1}$ in an isothermal 3 electrode half-cell configuration (Fig. S4a, ESI†). However, the introduction of this galvanic couple into an aqueous solution of PEDOT:PSS resulted in a liquid-state TG cell demonstrating a $S_i$ of $-2.52$ mV $K^{-1}$ (Fig. S4b, ESI†). The $S_i$, defined as $\left(S_i = \Delta V/\Delta T = -\dfrac{V(T_H) - V(T_C)}{T_H - T_C}\right)$, represents the negative ratio of the induced thermovoltage to the applied temperature difference (Fig. 1d). The reversibility of the electrochemical reactions within the polymer complex, PEDOT:PSS/$Fe(ClO_4)_{2/3}$, was verified *via* cyclic voltammetry analysis (Fig. S5, ESI†).[29] Given the comparable thermal mobility of cations and anions in solution, the observed $S_i$ originates exclusively from the TG effect. The recorded higher thermopower in the liquid-state TG cell ($-2.52$ mV $K^{-1}$) compared to the temperature coefficient in the isothermal half-cell (1.48 mV $K^{-1}$) is attributed to the increased molar entropy ($S_i$) difference, driven by electrostatic interactions between PEDOT:PSS and the $Fe^{2+/3+}$ ions. The $Fe^{3+}$ ions, possessing a higher charge density, engage in more substantial interactions with the sulfonate groups of PEDOT:PSS than $Fe^{2+}$ ions, resulting in a decreased $S_i$ for $Fe^{3+}$ ions (Fig. S6, ESI†). Furthermore, the acidic nature of PEDOT:PSS prevented the hydrolysis of $Fe^{2+/3+}$ into $Fe(OH)^+/^{2+}$, thereby preserving the charges of redox species, which proves advantageous in determining reaction entropy (Fig. S7, ESI†). This finding of a thermopower of $-2.52$ mV $K^{-1}$ significantly surpasses previously reported thermopower values in TG cells utilizing $Fe^{2+/3+}$ redox couples.[14,30]

The $S_i$ of the solid-state TD-assisted TG cells exhibited significant enhancement as the concentration of $Fe(ClO_4)_{2/3}$ increased, achieving an optimal value of $-40.05$ mV $K^{-1}$ at a concentration of 0.3 M (Fig. 1e). In contrast, the pristine PEDOT:PSS displayed a positive $S_i$ value of 27 mV $K^{-1}$, primarily due to the thermally driven diffusion of dissociated protons. The observed shift to a negative $S_i$ value in the solid-state TD-assisted TG cells is primarily due to the interactions between the $PSS^-$ and the $Fe^{2+/3+}$ ions, which promote the diffusion of $ClO_4^-$ counterions. In parallel, the $Fe(ClO_4)_{2/3}$ that does not engage in interactions with the sulfonate groups undergoes a galvanic reaction, contributing to the generation of electrochemical potential and faradaic currents.

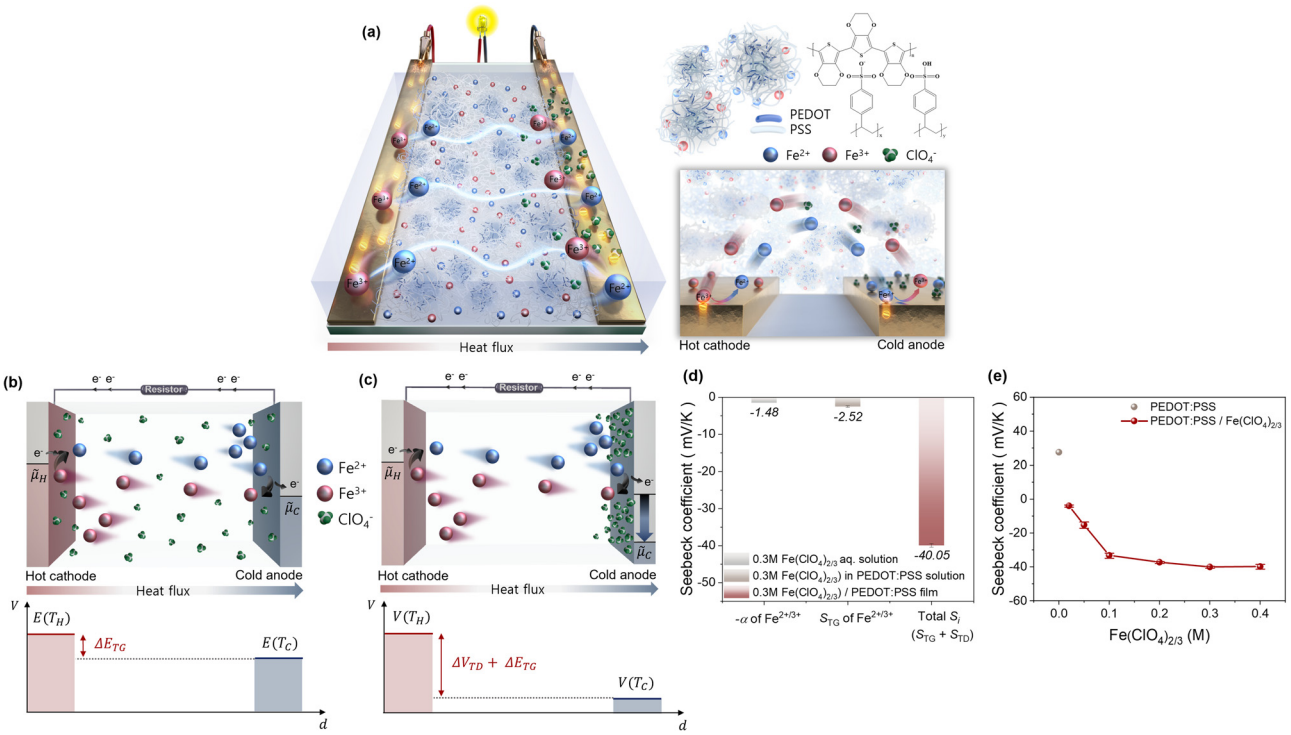


Fig. 1 Operational principle and thermopower of the solid-state TD-assisted TG cell. (a) The operational principle of the solid-state TD-assisted TG cell using PEDOT:PSS with the $Fe(ClO_4)_{2/3}$ galvanic couple. The enlarged view in the solid box highlights the reversible redox reactions of $Fe^{2+/3+}$ and the thermodiffusion of $ClO_4^-$ through ionic conduction channels within the PEDOT:PSS. (b) and (c) The electrode potential (b), ($E(T)$), arose from the electrochemical potential ($\tilde{\mu}_T$) caused by the redox reaction of $Fe^{2+/3+}$, ($E^0(T)$), while the electromotive force (c), ($V(T)$), concurrently induced by the thermodiffusion of $ClO_4^-$. (d) Partial contributions of temperature coefficient ($\alpha$) of $Fe^{2+/3+}$ and thermopower originated from the TG effect and thermodiffusion effect to the $S_i$ in solid-state TD-assisted TG cells. (e) The sign conversion of the $S_i$ in the PEDOT:PSS film with increasing concentrations of $Fe(ClO_4)_{2/3}$ from 0 to 0.4 M at 80% relative humidity.

To further substantiate the ionic interactions between the sulfonate groups and the $Fe^{2+/3+}$ ions, X-ray photoelectron spectroscopy (XPS) and Raman spectroscopy analyses were conducted. The XPS spectra revealed three primary O 1s peaks, associated with oxygen atoms in $PSS^-$ and $ClO_4^-$ (Fig. S8, ESI†). With an increase in $Fe(ClO_4)_{2/3}$ concentration, the O 1s peak related to $PSS^-$ at ~531.9 eV shifted to higher energies, while the Fe 2p peaks moved to lower energies (Fig. S9, ESI†).[31] These shifts suggest a decrease in the electron density of the oxygen atoms within $PSS^-$ due to their interaction with $Fe^{2+/3+}$ ions. Similarly, Raman spectra indicated that the addition of $Fe(ClO_4)_{2/3}$ led to a shift in the characteristic vibrational mode of the PEDOT moiety from 1437 $cm^{-1}$ to 1453 $cm^{-1}$ (Fig. S10, ESI†). This shift signifies the binding of Fe cations to sulfonate groups, reducing the coulombic interaction between the positively charged PEDOT and the negatively charged PSS, thereby partially dedoping PEDOT to a neutral benzoid structure.[31,32] These findings underscore that the incorporation of $Fe(ClO_4)_{2/3}$ into PEDOT:PSS facilitates the dissociation of $ClO_4^-$ counterions due to the interaction between $Fe^{2+/3+}$ ions and PSS units, enhancing the negative $S_i$ value as the concentration of $Fe(ClO_4)_{2/3}$ increases, driven by their thermodiffusion characteristics.

The notable increase in the $S_i$ of our TD-assisted TG cells, from −2.52 mV $K^{-1}$ to −40.05 mV $K^{-1}$, is primarily attributed to the diffusion of dissociated chaotropic ions ($ClO_4^-$) towards the colder electrode and their subsequent accumulation (Fig. S11, ESI†). This process elevates the Eastman entropy of transfer ($\hat{S}_i$),[33–35] which significantly amplifies the $S_i$ of the TD-assisted TG cells. The exceptional negative thermopower (n-type) observed in our TD-assisted TG cell is a consequence of the accumulated electric field created by both the electrochemical potential and the electromotive force, oriented in the same direction. This achievement is facilitated by the strategic use of the PEDOT:PSS matrix, which selectively interacts with the cationic components of the galvanic couple. It's noteworthy that this represents the first instance of an n-type TG cell achieving such a high level of thermopower. This dramatic enhancement contrasts with prior studies, where the larger ionic radius and mass of anions, compared to their counter cations, resulted in increased interactions with their environment. These interactions effectively hindered the diffusion of anions, limiting the n-type thermopower to values not exceeding −8.18 mV $K^{-1}$.[19]

The chaotropic characteristics of $ClO_4^-$ ions are substantiated through the analysis of O–H stretching modes within the FT-IR spectra of the polymer complex. In the spectra, typical O–H peaks associated with hydrogen bonding in water were identified at ~3230 $cm^{-1}$ (indicating strong hydrogen bonds) and 3355 $cm^{-1}$ (indicating weak hydrogen bonds). However, the introduction of $Fe(ClO_4)_{2/3}$ into the aqueous solution of

 

PEDOT:PSS resulted in a noticeable decrease in the intensity of these characteristic water peaks (Fig. S12, ESI†). Concurrently, a new, broad peak emerged at around ~3577 $cm^{-1}$. This newly observed peak is indicative of the coordination of $ClO_4^-$ ions with non-hydrogen-bonded water molecules, implying a significant disruption of the water network traditionally structured through hydrogen bonds. Notably, an increase in $Fe(ClO_4)_{2/3}$ concentration correlates with a rise in the intensity of the peak associated with non-hydrogen bonded water, further highlighting the chaotropic effect of $ClO_4^-$ ions.

To delve deeper into the influence of the kosmotropic/chaotropic nature of counter anions on the $\hat{S}_i$, a comparative analysis was conducted using galvanic couples based on $Fe^{2+/3+}$ with different counter anions ($FeCl_{2/3}$ and $Fe(SO_4)/Fe_2(SO_4)_3$). Solutions containing $Fe(SO_4)/Fe_2(SO_4)_3$ exhibited a pronounced enhancement of the hydrogen bonding peak at ~3230 $cm^{-1}$ as the concentration of $SO_4^{2-}$ increased, showcasing their kosmotropic behavior. Conversely, for PEDOT:PSS solutions containing $FeCl_{2/3}$, changes in the hydrogen bonding peak were minimal with increased $Cl^-$ concentration, indicating a less distinct nature of these counter anions.[6,14,30] The $S_i$ of PEDOT:PSS/$Fe(SO_4)/Fe_2(SO_4)_3$ was measured to be −3 mV $K^{-1}$ (at 0.3 M), attributable to the kosmotropic effect of the anions, while the $S_i$ of PEDOT:PSS/$FeCl_{2/3}$ was −7.35 mV $K^{-1}$ (at 0.1 M), reflecting a neutral nature (Fig. 2a). These results underscore that the exceptionally high $S_i$ value of −40.05 mV $K^{-1}$ for PEDOT:PSS/$Fe(ClO_4)_{2/3}$ is a direct consequence of the strong chaotropic nature of $ClO_4^-$ ions, thereby emphasizing the critical role of ion characteristics in modulating thermopower within TD-assisted TG cells.

### Output power

The maximum power density output ($P_{max}$) of TD-assisted TG cells was calculated using the formula $P_{max}/(\Delta T)^2 = V_{OC}J_{SC}/(2\Delta T)^2$, where $V_{OC}$ represents the open-circuit voltage, $J_{SC}$ denotes the short-circuit current density, and $\Delta T$ signifies the temperature difference across the cell. The peak output current density ($J_{max}$) of the TD-assisted TG cells showed enhancement with increasing concentration of $Fe(ClO_4)_{2/3}$. This improvement is largely attributed to the faradaic currents generated by the $Fe^{2+/3+}$ redox couple. Specifically, as the $Fe^{2+/3+}$ concentration in the polymer matrix was elevated, a corresponding increase in $J_{max}$ was observed, achieving a value of 5.6 A $m^{-2}$ $K^{-1}$ at a $Fe^{2+/3+}$ concentration of 0.3 M (Fig. 2b). The presence of excess galvanic couples predominantly drives the electrochemical reaction. In addition, since humidity can influence the degree of ion dissociation, its effect on output power performance is

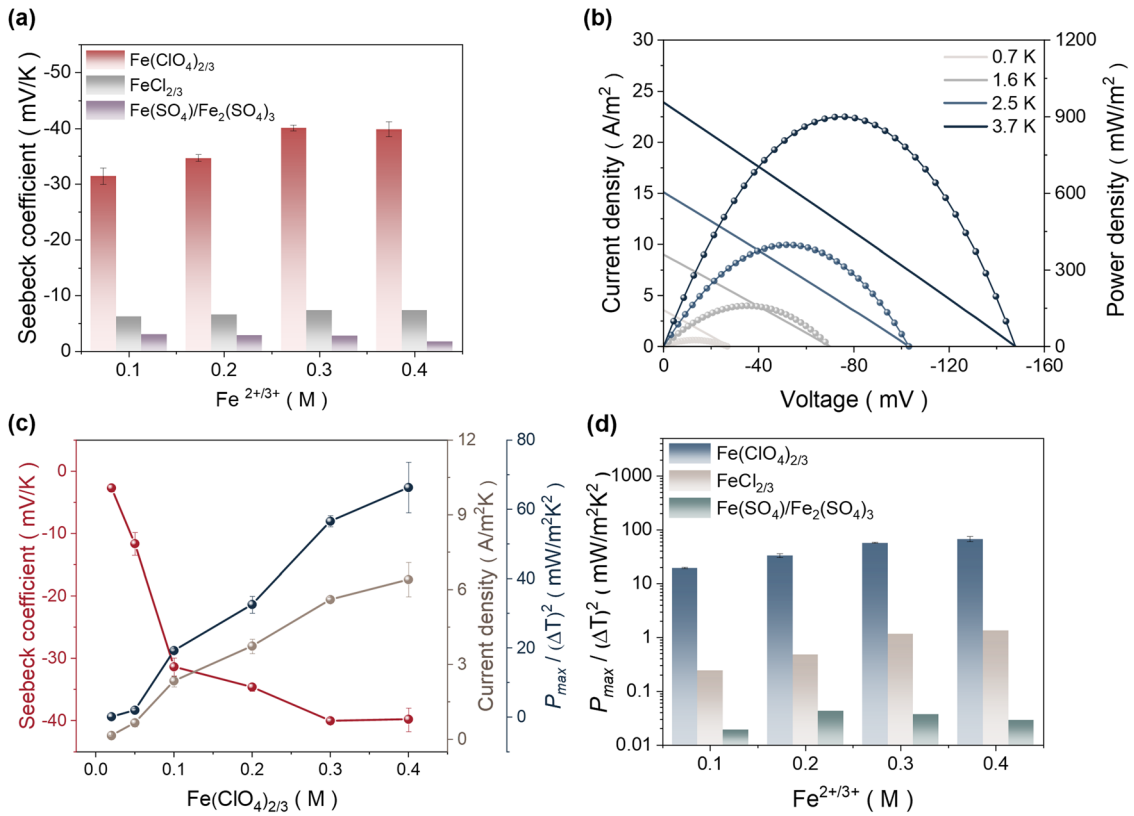


Fig. 2 Solid-state TD-assisted TG cells with various $Fe^{2+/3+}$ galvanic couples. (a) Comparative analysis of the $S_i$ using $Fe^{2+/3+}$ galvanic couples with different counter anions ($Fe(ClO_4)_{2/3}$, $FeCl_{2/3}$ and $Fe(SO_4)/Fe_2(SO_4)_3$) in PEDOT:PSS. (b) Peak output current density of PEDOT:PSS/$Fe(ClO_4)_{2/3}$ (0.3 M) under various temperature differences. (c) $S_i$, maximum output current density ($J_{max}$), and maximum output power density ($P_{max}$) normalized by the $\Delta T^2$ of PEDOT:PSS/$x$ M $Fe(ClO_4)_{2/3}$. (d) $P_{max}$ normalized by the $\Delta T^2$ of solid-state TD-assisted TG cells using $Fe(ClO_4)_{2/3}$, $FeCl_{2/3}$ and $Fe(SO_4)/Fe_2(SO_4)_3$ in the PEDOT:PSS film. All measurements were conducted under 80% relative humidity.

demonstrated in Fig. S13 (ESI†).[36] Moreover, the $P_{max}$ of the polymer complex, containing 0.3 M $Fe(ClO_4)_{2/3}$ and normalized by the $\Delta T^2$, achieved a value of 56.57 mW $m^{-2}$ $K^{-2}$ (Fig. 2c). Notably, this normalized $P_{max}$ value of 56.57 mW $m^{-2}$ $K^{-2}$ remarkably surpasses those of previously reported TG cells, as referenced in Table S2 (ESI†),[9,11–27,30,37–43] indicating a significant advancement in TG cell performance (Fig. 2d).

### Quasi-continuous operation

The TD-assisted TG cell is capable of operating in a quasi-continuous mode, enabled by a transient connection in the circuit where the temperature gradient is maintained (Fig. S14, ESI†). Initially, under open-circuit conditions, the cell is thermally charged, generating a thermovoltage due to the temperature gradient. Upon closing the circuit, the cell discharges across the external circuit, delivering maximum output currents, while the thermovoltage swiftly declines to 0 V. Remarkably, disconnecting the circuit while maintaining the applied temperature difference recharges the cells, facilitating multiple operating cycles. This recharging capability hinges on the ability of the redox couple to deplete the equilibrated electrical charges with the thermally diffused ions at the electrodes, thereby regenerating the thermovoltage (Fig. 3a).

The TD-assisted TG cell, upon being thermally charged with a temperature gradient of 1.7 K, generated a thermovoltage of ~70 mV and successfully completed 50 charge–discharge cycles within a span of 3 hours, as depicted in Fig. 3b. Throughout these cycles, the thermovoltage exhibited remarkable stability, with only a minor decrease of less than 14%. However, the $P_{max}$ tended to decrease as the operating cycles progressed, primarily

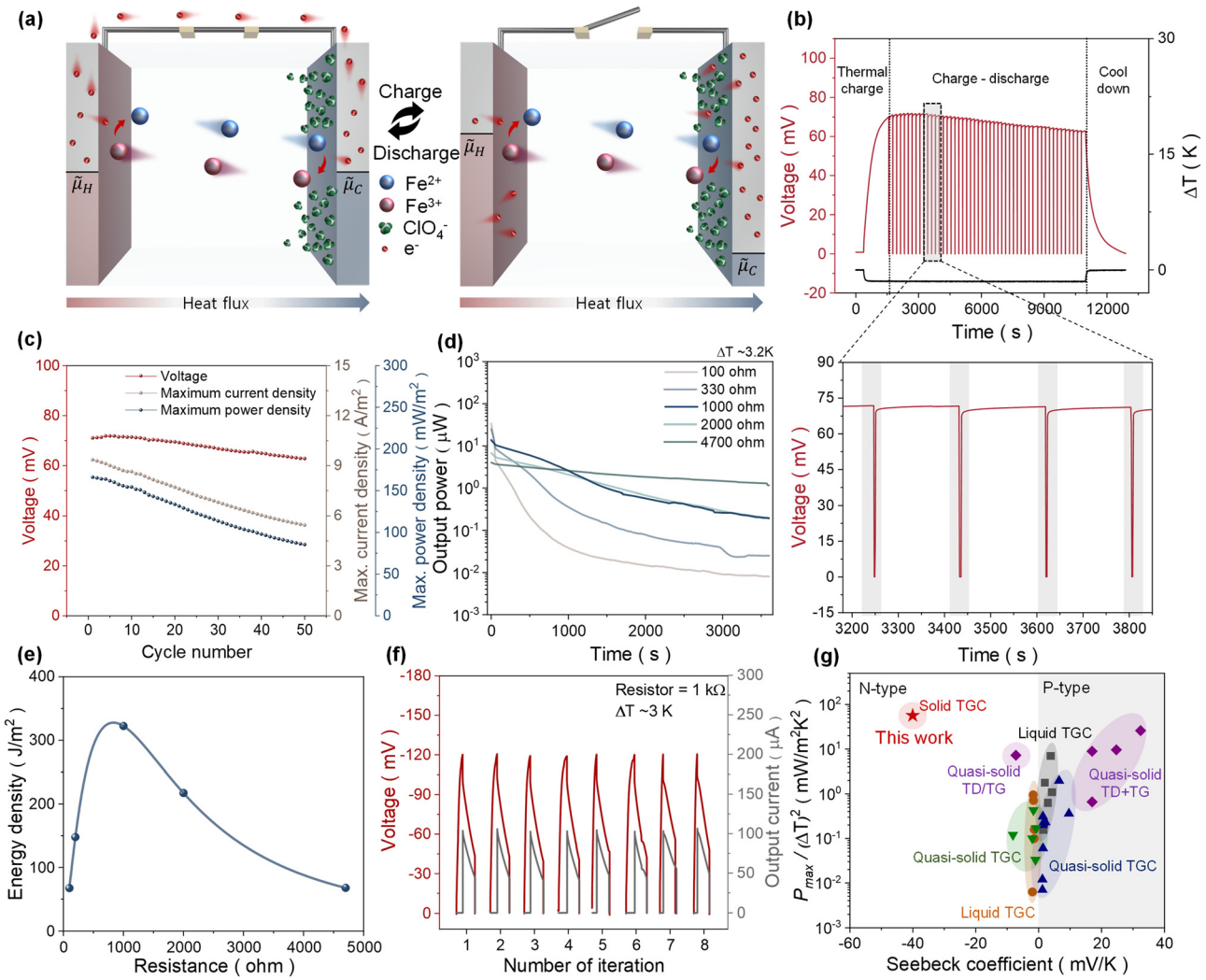


Fig. 3 Quasi-continuous operation and performance metrics. (a) Schematic illustration of a quasi-continuous operation of the solid-state TD-assisted TG cell *via* a transient circuit connection while maintaining the applied temperature gradients. (b) Thermovoltage during the 50 charge–discharge cycles. The enlarged graph in the dashed box shows the regeneration of thermovoltage upon disconnecting the circuit. (c) Thermovoltage, $J_{max}$, and $P_{max}$ of PEDOT:PSS/$Fe(ClO_4)_{2/3}$ (0.3 M) during 50 charge–discharge cycles. (d) and (e) Output power (d) and energy density (e) of PEDOT:PSS/$Fe(ClO_4)_{2/3}$ (0.3 M) in continuous operation using different resistors. (f) Consistent restoration of the initial $P_{out}$ through 8 iterations. (g) Performance comparison ($P_{max}/(\Delta T)^2$ and $S_i$) of TG cells reported in the literature. Data is categorized based on the working principle (n-type or p-type).

 

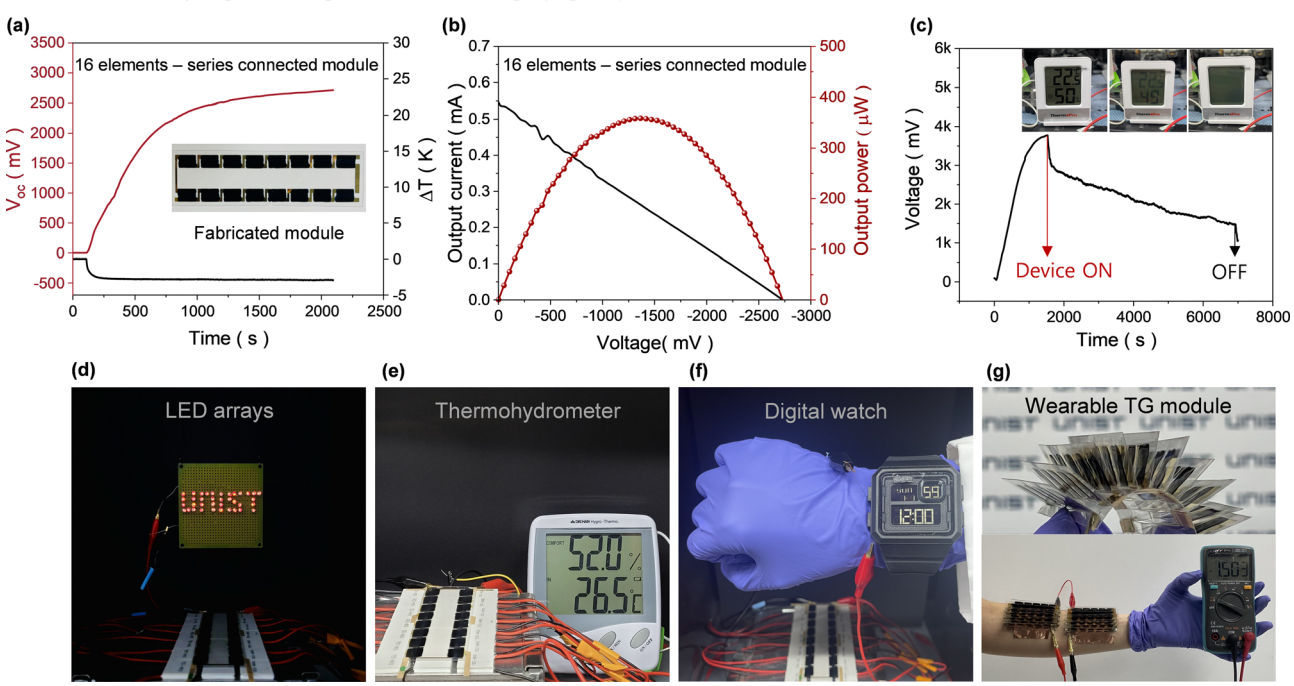


Fig. 4 Demonstration of practical applications using the serially connected TG modules. (a) and (b) Thermovoltage (a) and output power (b) of the module with 16 elements of PEDOT:PSS/$Fe(ClO_4)_{2/3}$ (0.3 M). (c) Module powering a commercial thermohydrometer continuously for over 90 min. (d)–(f) Direct operation of commercial electronic devices such as LED arrays (d), a thermohydrometer (e), and a digital watch (f). (g) A wearable module fabricated in a Lego-like configuration with 100 serially connected elements, harvesting natural body heat.

due to a reduction in the $J_{max}$ (Fig. 3c). In scenarios where the external resistor was engaged for continuous operation, the $P_{out}$ initially experienced a decline before stabilizing at a steady state. This steady state was characterized by the thermovoltage generated solely from the electrochemical reaction (Fig. 3d). An energy density of 322.4 J $m^{-2}$ was achieved using a 1000-Ohm resistor over the course of 1 hour (Fig. 3e). This decline can be attributed to electrode polarization, which arises from the accumulation of $ClO_4^-$ ions, thereby hindering the access of galvanic reactants to the electrode surfaces for subsequent electrochemical reactions. To mitigate these challenges, the cell was resumed by removing the temperature gradient, enabling the uniform redistribution of ions to initiate the next iteration of the process. As shown in Fig. 3f, the initial $P_{out}$ was consistently restored across eight full charge–discharge iterative processes, supporting the feasibility of continuous operation over extended periods.

The evaluation of thermal energy conversion efficiency in thermoelectric devices, including TG cells, is commonly benchmarked against the Carnot-relative efficiency ($\eta_r$), which provides a universal criterion for assessing performance. The TD-assisted TG cell demonstrated a $\eta_r$ of 0.242% near room temperature (Table S3, ESI†). When the performance of the TD-assisted TG cell is juxtaposed with other reported n-type TG cells, its achieved $\eta_r$ and $P_{max}$ is notably superior, as illustrated in Fig. 3g (Table S2, ESI†). Despite the operational functionality of the developed TD-assisted TG cell being transient, primarily due to cell polarization, the remarkable thermal-to-electrical energy conversion efficiency underscores the potential of advanced TG cells in thermoelectric applications, suggesting avenues for further optimization and enhancement of their energy conversion processes.

### Practical operation of commercial devices by TG module

We developed a TG module comprising 16 TD-assisted TG cells that were serially connected (Fig. S15, ESI†). At a temperature gradient of ~4 K, the module was able to generate a thermovoltage of 2.71 V and a short-circuit current of 540 μA, as shown in Fig. 4a. This module achieved an output power of ~360 μW (Fig. 4b). Additionally, it was capable of powering a commercial thermohydrometer continuously for over 90 minutes under a temperature gradient of ~5 K (Fig. 4c). The considerable $P_{out}$ of our module enables it to directly power commercial devices such as a light-emitting diode (LED) array, a thermohydrometer, and a digital watch, all without the need for a voltage booster. This capability is illustrated in Fig. 4d–f.

Additionally, we ventured into the realm of wearable technology by constructing a device consisting of 100 elements serially connected in a Lego-like configuration. This wearable device successfully harvested low-grade body heat to produce an output voltage of 1.5 V, showcased in Fig. 4g. These practical demonstrations highlight the significant potential of our TG module for application in wearable devices. They underscore our belief that the strategic integration in our TD-assisted TG cell represents a crucial advancement in the field of thermal energy harvesting. This approach not only showcases the capability of such materials in efficiently converting thermal energy into electrical energy but also paves the way for their application in a wide range of wearable and portable

electronics, marking a significant stride towards sustainable energy solutions.

## Conclusions

This study presents the development and characterization of the first-time solid-state n-type TD-assisted TG cell leveraging a PEDOT:PSS/$Fe(ClO_4)_{2/3}$ polymer complex. The optimized cell demonstrates a significantly enhanced thermopower of $-40.05$ mV $K^{-1}$ at 0.3 M concentration of $Fe(ClO_4)_{2/3}$, setting a new benchmark for n-type TG cells. This achievement is largely attributed to the dual functionality of the galvanic couple in our TD-assisted TG cell, which synergistically advances both electrochemical reactions through $Fe^{2+/3+}$ and thermodiffusion *via* the liberated $ClO_4^-$ ions within a polymer complex. The cell exhibited a maximum power density far surpassing previously reported TG cells, with a Carnot-relative efficiency of 0.242% near room temperature. Such performance highlights the potential of our TD-assisted TG cell in thermal energy conversion applications. Further innovations were demonstrated through the construction of a TG module consisting of 16 serially connected cells, achieving a substantial output power capable of directly powering commercial electronic devices such as LED arrays, thermohydrometers, and digital watches without the need for voltage boosters. Moreover, a wearable device configuration comprising 100 elements serially connected in a Lego-like configuration showcased the feasibility of harvesting low-grade body heat, producing an output voltage of 1.5 V. The innovative approach demonstrated in this work not only advances our understanding of ionic thermoelectric materials but also serves as a pivotal step towards realizing sustainable and efficient energy conversion technologies, marking a significant contribution to the field of thermal energy harvesting.

## Author contributions

S.-Y. J. and J.-Y. B. conceived this work. J.-Y. B. developed the methodology, performed the experiments, and analyzed the data. H. J. S. prepared the schematic illustration. S.-Y. J. directed and supervised the project. The manuscript was written by S.-Y. J. and J.-Y. B.

## Data availability

All data are included in this published article and its ESI.†

## Conflicts of interest

There are no conflicts to declare.

## Acknowledgements

This work was supported by the Ministry of Education of the Republic of Korea and the National Research Foundation of Korea (NRF) grant funded by the Korean government (MSIP) (2023R1A2C3002881 and RS-2023-00222006). The authors acknowledge the support from UNIST Central Research Facilities (UCRF) and the Korea Institute of Materials Science (KIMS).

## References

1 J. P. Heremans, *Nature*, 2014, **508**, 327–328.
2 T. I. Quickenden and Y. Mua, *J. Electrochem. Soc.*, 1995, **142**, 3985.
3 R. Zito, *AIAA J.*, 1963, **1**, 2133–2138.
4 A. J. deBethune, T. S. Licht and N. Swendeman, *J. Electrochem. Soc.*, 1959, **106**, 616.
5 T. Migita, N. Tachikawa, Y. Katayama and T. Miura, *Electrochemistry*, 2009, **77**, 639–641.
6 J. T. Hupp and M. J. Weaver, *Inorg. Chem.*, 1984, **23**, 3639–3644.
7 S. Sahami and M. J. Weaver, *J. Electroanal. Chem. Interfacial Electrochem.*, 1981, **122**, 171–181.
8 R. H. Hammond and W. M. Risen, *Sol. Energy*, 1979, **23**, 443–449.
9 B. Yu, J. Duan, H. Cong, W. Xie, R. Liu, X. Zhuang, H. Wang, B. Qi, M. Xu, Z. L. Wang and J. Zhou, *Science*, 2020, **370**, 342–346.
10 B. Burrows, *J. Electrochem. Soc.*, 1976, **123**, 154.
11 B. Yu, H. Xiao, Y. Zeng, S. Liu, D. Wu, P. Liu, J. Guo, W. Xie, J. Duan and J. Zhou, *Nano Energy*, 2022, **93**, 106795.
12 J. Duan, G. Feng, B. Yu, J. Li, M. Chen, P. Yang, J. Feng, K. Liu and J. Zhou, *Nat. Commun.*, 2018, **9**, 5146.
13 T. Kim, J. S. Lee, G. Lee, H. Yoon, J. Yoon, T. J. Kang and Y. H. Kim, *Nano Energy*, 2017, **31**, 160–167.
14 K. Kim, S. Hwang and H. Lee, *Electrochim. Acta*, 2020, **335**, 135651.
15 L. Liu, D. Zhang, P. Bai, Y. Mao, Q. Li, J. Guo, Y. Fang and R. Ma, *Adv. Mater.*, 2023, **35**, 2300696.
16 W. Gao, Z. Lei, W. Chen and Y. Chen, *ACS Nano*, 2022, **16**, 8347–8357.
17 Z. Lei, W. Gao, W. Zhu and P. Wu, *Adv. Funct. Mater.*, 2022, **32**, 2201021.
18 S. Pu, Y. Liao, K. Chen, J. Fu, S. Zhang, L. Ge, G. Conta, S. Bouzarif, T. Cheng, X. Hu, K. Liu and J. Chen, *Nano Lett.*, 2020, **20**, 3791–3797.
19 Y. Han, J. Zhang, R. Hu and D. Xu, *Sci. Adv.*, 2022, **8**, eabl5318.
20 P. Yang, K. Liu, Q. Chen, X. Mo, Y. Zhou, S. Li, G. Feng and J. Zhou, *Angew. Chem., Int. Ed.*, 2016, **55**, 12050–12053.
21 Y. Liu, S. Zhang, Y. Zhou, M. A. Buckingham, L. Aldous, P. C. Sherrell, G. G. Wallace, G. Ryder, S. Faisal, D. L. Officer, S. Beirne and J. Chen, *Adv. Energy Mater.*, 2020, **10**, 2002539.
22 C.-G. Han, X. Qian, Q. Li, B. Deng, Y. Zhu, Z. Han, W. Zhang, W. Wang, S.-P. Feng, G. Chen and W. Liu, *Science*, 2020, **368**, 1091–1098.
23 Y. Li, Q. Li, X. Zhang, B. Deng, C. Han and W. Liu, *Adv. Energy Mater.*, 2022, **12**, 2103666.
24 Y. Li, Q. Li, X. Zhang, J. Zhang, S. Wang, L. Lai, K. Zhu and W. Liu, *Energy Environ. Sci.*, 2022, **15**, 5379–5390.
25 W. Gao, Z. Lei, C. Zhang, X. Liu and Y. Chen, *Adv. Funct. Mater.*, 2021, **31**, 2104071.

 

26 X. Shi, L. Ma, Y. Li, Z. Shi, Q. Wei, G. Ma, W. Zhang, Y. Guo, P. Wu and Z. Hu, *Adv. Funct. Mater.*, 2023, **33**, 2211720.
27 C. Xu, Y. Sun, J. Zhang, W. Xu and H. Tian, *Adv. Energy Mater.*, 2022, **12**, 2201542.
28 D. Zhang, Y. Mao, F. Ye, Q. Li, P. Bai, W. He and R. Ma, *Energy Environ. Sci.*, 2022, **15**, 2974–2982.
29 J. H. Kim, J. H. Lee, R. R. Palem, M.-S. Suh, H. H. Lee and T. J. Kang, *Sci. Rep.*, 2019, **9**, 8706.
30 M. A. Buckingham, F. Marken and L. Aldous, *Sustainable Energy Fuels*, 2018, **2**, 2717–2726.
31 B. Kim, J. U. Hwang and E. Kim, *Energy Environ. Sci.*, 2020, **13**, 859–867.
32 J. Ouyang, C. W. Chu, F. C. Chen, Q. Xu and Y. Yang, *Adv. Funct. Mater.*, 2005, **15**, 203–208.
33 E. D. Eastman, *J. Am. Chem. Soc.*, 1928, **50**, 283–291.
34 J. N. Agar, C. Y. Mou and J. L. Lin, *J. Phys. Chem.*, 1989, **93**, 2079–2082.
35 K. I. Assaf and W. M. Nau, *Angew. Chem., Int. Ed.*, 2018, **57**, 13968–13981.
36 Z. A. Akbar, J.-W. Jeon and S.-Y. Jang, *Energy Environ. Sci.*, 2020, **13**, 2915–2923.
37 M. Yang, Y. Hu, X. Wang, H. Chen, J. Yu, W. Li, R. Li and F. Yan, *Adv. Mater.*, 2024, **36**, 2312249.
38 L. Zhang, T. Kim, N. Li, T. J. Kang, J. Chen, J. M. Pringle, M. Zhang, A. H. Kazim, S. Fang, C. Haines, D. Al-Masri, B. A. Cola, J. M. Razal, J. Di, S. Beirne, D. R. MacFarlane, A. Gonzalez-Martin, S. Mathew, Y. H. Kim, G. Wallace and R. H. Baughman, *Adv. Mater.*, 2017, **29**, 1605652.
39 J. Hu, J. Wei, J. Li, L. Bai, Y. Liu and Z. Li, *Energy Environ. Sci.*, 2024, **17**, 1664–1676.
40 L. Jin, G. W. Greene, D. R. MacFarlane and J. M. Pringle, *ACS Energy Lett.*, 2016, **1**, 654–658.
41 H. Im, T. Kim, H. Song, J. Choi, J. S. Park, R. Ovalle-Robles, H. D. Yang, K. D. Kihm, R. H. Baughman, H. H. Lee, T. J. Kang and Y. H. Kim, *Nat. Commun.*, 2016, **7**, 10600.
42 Y. Liu, Q. Zhang, G. O. Odunmbaku, Y. He, Y. Zheng, S. Chen, Y. Zhou, J. Li, M. Li and K. Sun, *J. Mater. Chem. A*, 2022, **10**, 19690–19698.
43 H. Zhou, T. Yamada and N. Kimizuka, *J. Am. Chem. Soc.*, 2016, **138**, 10502–10507.